ACS OMEGA

http://pubs.acs.org/journal/acsodf

Article

Facile Synthesis of Self-Assembled NiFe Layered Double Hydroxide-Based Azobenzene Composite Films with Photoisomerization and Chemical Gas Sensor Performances

Ying He, Ran Wang, Chenguang Sun, Shufeng Liu, Jingxin Zhou, Lexin Zhang,* Tifeng Jiao,* and Qiuming Peng

Cite This: *ACS Omega* 2020, 5, 3689−3698

Read Online

ACCESS | Metrics & More | Article Recommendations

ABSTRACT: Two kinds of layered double hydroxide (LDH) Langmuir composite films containing azobenzene (Azo) groups were successfully prepared by Langmuir−Blodgett (LB) technology. Then, an X-ray diffractometer (XRD), a transmission electron microscope (TEM), and an atomic force microscope (AFM) were used to investigate the structures of NiFe-LDH and the uniform morphologies of the composite LB films. The photoisomerization and acid−base gas sensor performances of the obtained thin film samples were tested by infrared visible (FTIR) spectroscopy and ultraviolet visible (UV−vis) spectroscopy. It is proved that the Azo dye molecules in the composite film are relatively stable to photoisomerization. In addition, the prepared composite films have high sensing sensitivity and good recyclability for acid−base response gases. The present research proposes a new clue for designing thin film materials for chemical gas response with good stability and sensitivity.

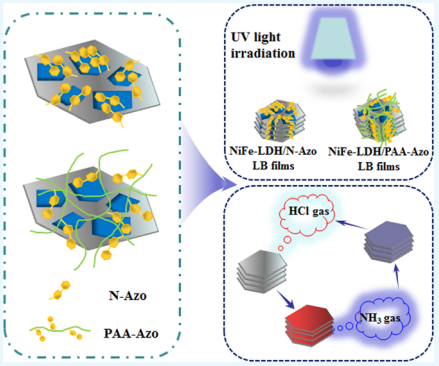

1. INTRODUCTION

In recent years, the rational design of various functionalized layered double hydroxide (LDH) nanocomposites has received increasing attention from researchers. To fully demonstrate the diverse applications of LDH materials, the surface can be functionalized.[1−3] LDH is widely used in catalytic materials, hydrogels, polymeric films, and other fields because of the two-dimensional configuration, indicating that it has good processability and practicality for nanomaterials.[4−8] According to reports, Wang et al. developed a self-assembled cross-linked LDH-doped nanocomposite hydrogel with excellent mechanical properties.[9] On the other hand, after the surface of LDH is modified, it can effectively combine with dye molecules to form polymers with gas selectivity. For example, it has been reported that the lanthanide cation was inserted into the LDH layer, and its potential applications in materials such as biomedical sensing and optoelectronic devices were studied.[10] It is worth noting that after the LDH layers are peeled into a positively charged nanosheet layer, an assembly unit is obtained for thin film materials.[11−14] Therefore, use of LDH units to build multilayer thin film materials seems to be an interesting challenge.

Azobenzene (Azo) dye molecules have been invented in1836. The color richness and photochromism of these compounds have attracted widespread interest.[15,16] They belongs to a class of organic dye molecules containing a N═N azo double bond structure. In the past 10 years, azo cross-linked materials have attracted significant attention, because such materials are expected to be applied in the fields of microdynamics, photoelectronics, photonics, and optical signal processing.[17−21] Azo-type materials can undergo trans−cis isomerization under appropriate lamp irradiation. As a photosensitive reaction material, it has been extensively studied, and this characteristic is also the most significant.[22] It has been mentioned in existing articles that this photoisomerization of Azo and its derivatives, as well as many other physical and chemical properties, originates from the nonlocality of π electrons. The trans−cis isomerization process for can be completed by either the $\pi-\pi^*$ energy level or the $n-\pi^*$ energy level.[23] In addition, there is a statement that azobenzene dyes form modified materials with polymers through doping or cross-linking. This material has a large optical nonlinear coefficient and is widely studied and applied in the fields of optoelectronics.[24−27] Other research teams have studied and characterized the inclusion formation of Azo compounds and β-cyclodextrin at the air−water interface.[28] Due to the photoisomerization of Azo dyes, their arrangement in polymers and a series of phenomena caused by photo-

Received: December 14, 2019
Accepted: January 30, 2020
Published: February 12, 2020

https://dx.doi.org/10.1021/acsomega.9b04290
ACS Omega 2020, 5, 3689−3698

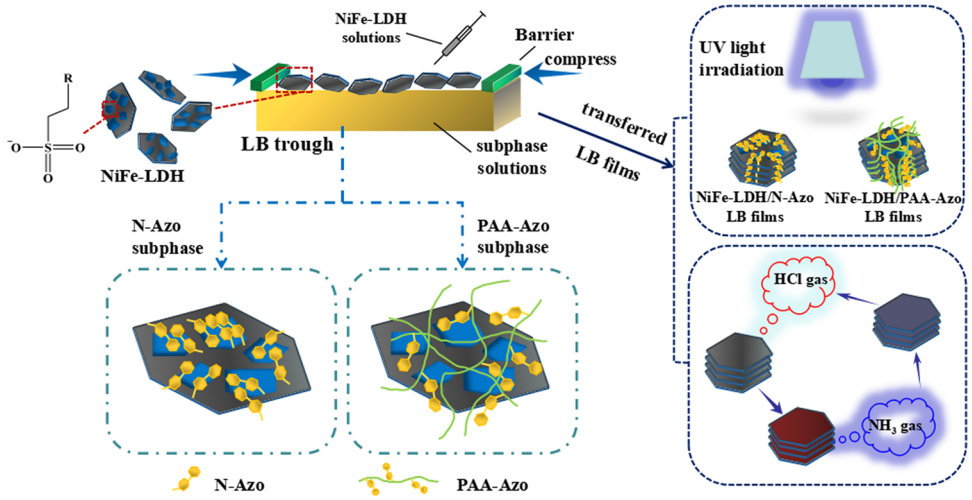

Figure 1. Scheme and characteristic tests of the preparation process of interfacial self-assembly of NiFe-LDH composite Langmuir films.

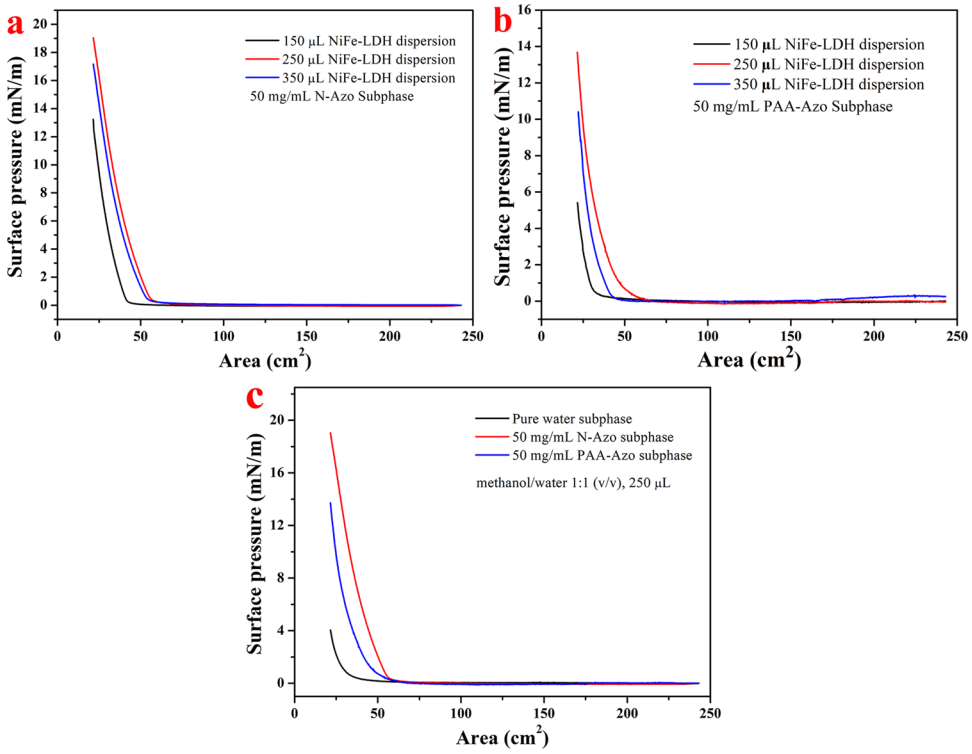

Figure 2. Surface pressure−area isotherm (π−A) of the synthesized NiFe-LDH Langmuir films: (a) N-Azo subphase, different volume dispersion; (b) PAA-Azo subphase, different volume dispersion; (c) different subphases (methanol/water (v/v) of 1:1, volume of 250 μL, concentration of 0.7 mg/mL).

isomerization have become the focus of research in recent years.

The present work uses Langmuir−Blodgett (LB) technology to effectively self-assemble the modified nickel−iron LDH (NiFe-LDH) sheet and azobenzene (Azo) compounds for synthesizing a large-scale interface with dense and uniform composite materials.[29] Interestingly, the obtained composite thin film materials will be particularly advantageous due to their excellent molecular recognition capabilities and modest self-assembled models. The results demonstrate that the reason for the formation of the current composite Langmuir films is hydrogen bonds and static electricity synergistic interaction between the groups used to modify NiFe-LDH and the soluble small molecules or polymer molecules containing Azo.[30] In addition, Langmuir films obtained by LB assembly technology can be easily transferred to solid substrates for characterization using morphological and spectral methods. Finally, these composite films were tested for photoisomerization stability and acid−base gas induction. The obtained results show that compared with the original sample solutions, after combining NiFe-LDH and azo dye into LB films, the composite films have reduced light sensitivity while the internal structures are not easily changed. NiFe-LDH plays a role in stably blocking ultraviolet light. In addition, the prepared composite films have high sensing sensitivity and good recyclability for acid−base response gases. Therefore, the prepared composite materials

https://dx.doi.org/10.1021/acsomega.9b04290
ACS Omega 2020, 5, 3689−3698

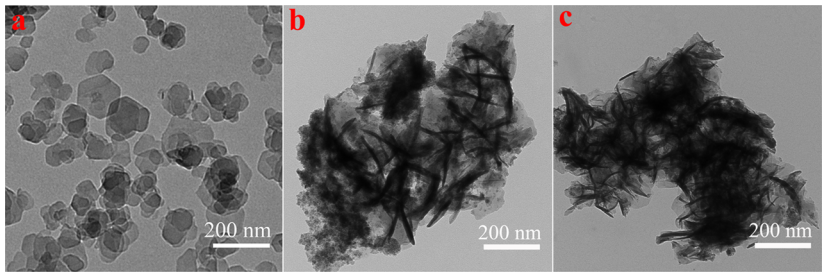

Figure 3. TEM images of NiFe-LDH sheets (a), NiFe-LDH/PAA-Azo LB film (b), and NiFe-LDH/N-Azo LB film (c).

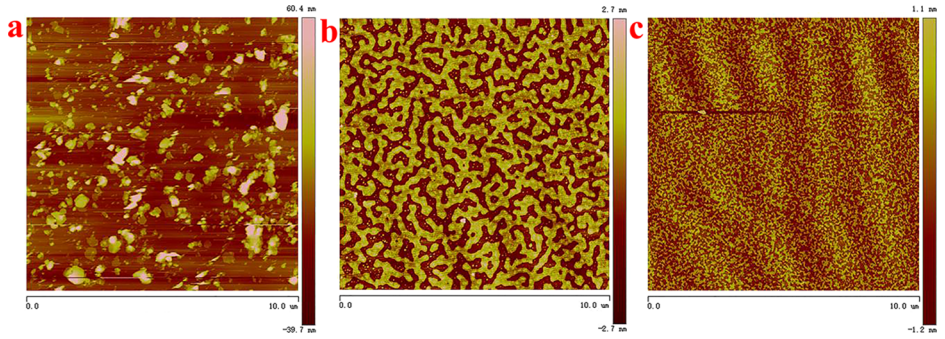

Figure 4. AFM images of NiFe-LDH sheets (a), NiFe-LDH/PAA-Azo LB film (b), and NiFe-LDH/N-Azo LB film (c).

provide important application prospects for the design of nano-optical devices and biochemical sensors.

2. RESULTS AND DISCUSSION

2.1. Preparation and Characterization of Langmuir Films. First, the self-assembly and characteristic test scheme of the NiFe-LDH composite Langmuir film was simply plotted. The initially prepared NiFe-LDH showed a hexagonal shape under the transmission electron microscopy (TEM), and it was replaced by a gray hexagonal sheet in this process. Through the LB system, NiFe-LDH was transferred to the surface of the subphase molecules using a microsyringe to fully disperse and react and then forming NiFe-LDH/PAA-Azo and NiFe-LDH/N-Azo Langmuir film, respectively. Subsequently, the film was transferred to different substrates. On the one hand, it was used to carry out the photoisomerization reaction by UV lamp irradiation. On the other hand, after the prepared composite film was exposed to the acid or base gas continuously, a cyclic acid−base response occurred. These characteristics indicate that the self-assembled LB composite films have good optical stability and gas sensitivity. It opens up new ideas for future research on optical switches, optical signal processors, chemical gas induction film materials, and other self-assembled nanocomposites (Figure 1).

To more conveniently select a reasonably quantitative diffusion solution volume and subphase solution, the surface pressure−spread area isothermal curves (π−A) of the self-assembled Langmuir composite films were demonstrated using the LB system. Prior to this, the polarity of the NiFe-LDH dispersion should be adjusted. The volume ratio of methanol/water = 1/1 is the most suitable dissolution ratio. As shown in Figure 2a, when N-Azo was selected as a single stationary subphase, the diffusion volume of the NiFe-LDH dispersion was changed (150, 250, and 350 μL), and three curves were obtained. It is obvious that the red curve has the highest initiation pressure and the largest collapse pressure that can be achieved. Figure 2b shows the same results as Figure 2a. Therefore, 250 μL of the diffusion solution was selected for subsequent LB film preparation. Next, Figure 2c is based on the selection of Figure 2a,b, and the dispersion is diffused to the surface of three different subphase solutions (pure aqueous solution, *p*-aminoazobenzene (N-Azo) solution, and polyacrylic acid-azobenzene (PAA-Azo) solution). It can be clearly seen that as the compression progresses, the curve is initially stable. At the trough area of about 60 cm^2, the isotherm gradually begins to show an upward trend. The curve starts very late in the pure water subphase solution, and the collapse pressure finally reached is very low, only 4 mN/m. This may be because of the fact that the polarity of the dispersion is similar to that of water. As the spreading diffusion time increases, some of it dissolves and the other sinks into the bottom of the aqueous solution, which is not conducive to the formation of the Langmuir film.[31,32] Therefore, in this research, we will not perform much analysis on the pure water subphase composite film. When N-Azo is used as a subphase solution, the surface pressure gradually increases at a trough area of 62 cm^2 and the final pressure increases to 19 mN/m. When the subphase is PAA-Azo, the surface pressure starts to increase when the trough area is also squeezed to about 62 cm^2. The difference is that the increase in speed is relatively slow, and the maximum pressure it can reach is 14 mN/m. The different changes of the π−A isotherm indicate that there are different interface interactions between the sulfate group in NiFe-LDH and the N-Azo or PAA-Azo molecules, which led to the formation of LB composite films.

To express the nanolevel morphology of the NiFe-LDH composite Langmuir film more clearly, a preliminary observation of the film was performed using a transmission electron microscope, as shown in Figure 3. First of all, it can be seen in Figure 3a that the pure NiFe-LDH hexagonal sheet structure is monodispersed with a size range of 50−150 nm. Compared with NiFe-LDH sheets (Figure 3a), NiFe-LDH/PAA-Azo (Figure 3b) and NiFe-LDH/N-Azo (Figure 3c) films show a wide range of cross-linked aggregates at the interface.

https://dx.doi.org/10.1021/acsomega.9b04290
ACS Omega 2020, 5, 3689−3698

Furthermore, atomic force microscopy (AFM) was also used to further investigate the surface of the single-layer Langmuir film, as shown in Figure 4. Figure 4a shows the disordered and irregular state of NiFe-LDH lamellae, whereas Figure 4b,c show uniform and dense NiFe-LDH/PAA-Azo and NiFe-LDH/N-Azo composite films. In particular, it is clearly seen in Figure 4b that the NiFe-LDH/PAA-Azo composite film has a uniform network-like region with uniform voids due to the surface extrusion of the LB system. A number of NiFe-LDH small-sized particles adhere to the inside of the void structure, forming small and uniform aggregates. Moreover, in Figure 4c, the NiFe-LDH/N-Azo composite film with a more minute size of voids and aggregates can be observed. In comparison, the network structure formed in the NiFe-LDH/PAA-Azo film may be the long alkyl chain of PAA introduced into the composite film.[28,33] These images also correspond to the composite film aggregates described in the TEM image. The R_a of the thin film in Figure 4b,c is 0.364 and 0.892 nm, respectively. These results are sufficient to indicate that the surface roughness of the films is small. Accordingly, these composite films exhibit different microscopic morphologies, which further illustrates that the Langmuir composite film can make NiFe-LDH sheets appear uniform and dense at the interface after being prepared. At the same time, there are some intermolecular forces between NiFe-LDH and PAA-Azo or N-Azo molecules, and different manifestations of azobenzene molecules have different mechanisms of action.

Figure 5 depicts the characterization of the prepared NiFe-LDH, PAA-Azo, and two LB multilayer composite films using an X-ray diffractometer, and the configurations of these materials are analyzed. Corresponding to the existing literature, after the surface of PAA was modified with azobenzene, it could be clearly seen that the initial strong diffraction peak at 2θ = 19.7° and the weak broad diffraction peak at 2θ = 37.2° respectively shifted to 23.5 and 43.1°.[28] From the Bragg equation $2d \sin\theta = n\lambda$ (λ = 1.54 Å), the angle of the diffraction peak is inversely proportional to the crystal plane spacing.[34] Therefore, the results indicated that the interlayer distance of molecules was reduced to some extent after the introduction of the Azo group. NiFe-LDH has a unique symbolic diffraction peak at 11.3°, and the diffraction crystal plane is (003), which proves that NiFe-LDH is successfully synthesized. Comparing the peaks of the NiFe-LDH/N-Azo and NiFe-LDH/PAA-Azo composite films, the peak of the (003) crystal plane almost disappeared, and the diffraction peaks between 2θ = 30 and 70° still exist and are sharp. This shows that NiFe-LDH does exist in the formed composite films,[35] and the interlayer distance after the formation of film has increased, which further proves that a uniform and dense void film has been observed in the atomic force image and also fully illustrates that the composite films are successfully synthesized.

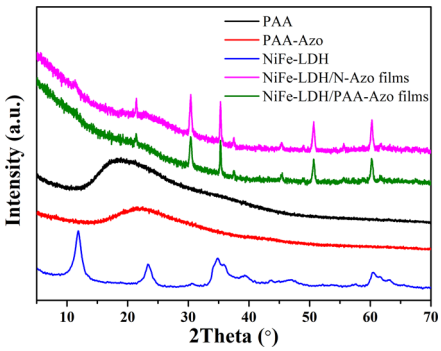

Figure 5. XRD of PAA, PAA-Azo, NiFe-LDH, NiFe-LDH/N-Azo LB film, and NiFe-LDH/PAA-Azo LB film.

Because the azo-phenyl group has a distinct characteristic absorption peak in the UV−vis spectrum, Figure 6a,b displays the spectra of the pure NiFe-LDH solution, the two original solutions, and the prepared composite films. The mechanism of interaction between azobenzene-containing substances and NiFe-LDH was further studied. From Figure 6a, it can be seen that the (trans isomer) $\pi-\pi^*$ transfer characteristic peak of the Azo group inside PAA-Azo is originally at 339 nm. After interacting with NiFe-LDH, the peak position shifted toward right to 354 nm. Similarly, in the NiFe-LDH/N-Azo composite film spectrum (Figure 6b), the assignment of the azo peak shifted toward right from 374 to 400 nm. Both types of composite films exhibited a red shift in the UV−vis spectra, which explains that the J-aggregates occurred between the conjugated Azo group and NiFe-LDH.[36]

For a further study of the interaction of NiFe-LDH with the azobenzene molecules in the subphase solution, the Fourier transform infrared (FTIR) spectra of the two LB composite films were characterized as shown in Figure 7. The band in the range of 3500−3200 cm^{-1} is ascribed to the stretching vibration of the intermolecular hydrogen bond O−H, which corresponds to 3425 cm^{-1} in the NiFe-LDH spectrum. At 1360 and 1630 cm^{-1}, the symmetrical and antisymmetric bending vibration absorption peaks of the S═O bond are

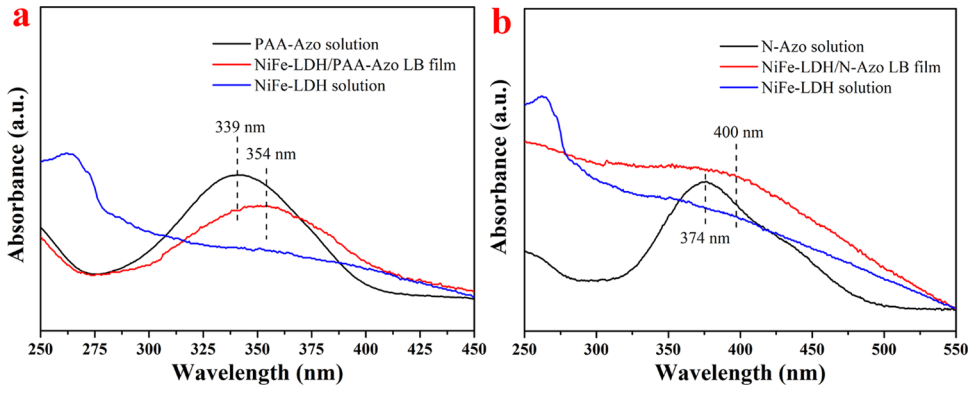

Figure 6. UV-vis spectra of NiFe-LDH/PAA-Azo (a) and NiFe-LDH/N-Azo LB films (b).

https://dx.doi.org/10.1021/acsomega.9b04290
ACS Omega 2020, 5, 3689−3698

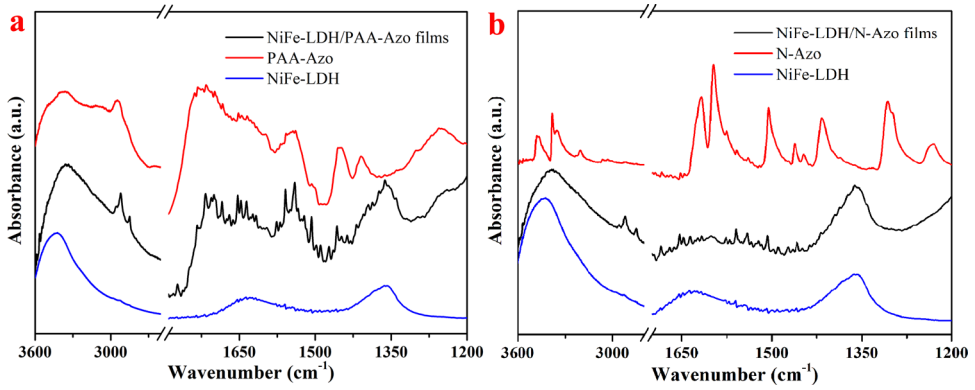

Figure 7. FTIR spectra of NiFe-LDH/PAA-Azo (a) and NiFe-LDH/N-Azo LB films (b).

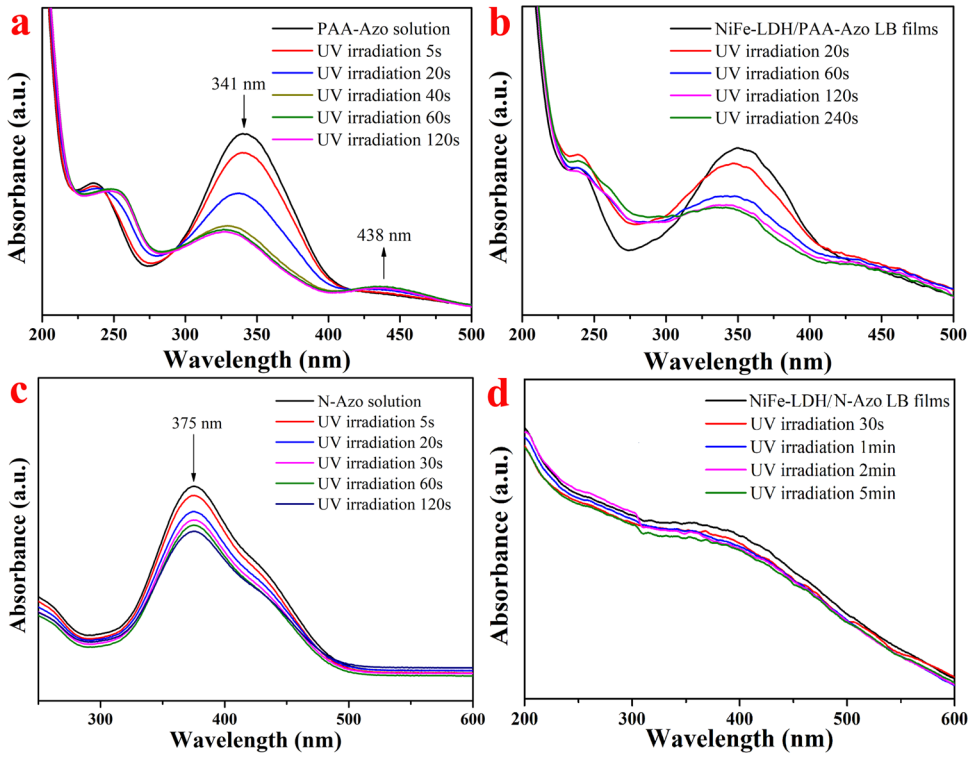

Figure 8. Changes in UV spectra of PAA-Azo (a), N-Azo solutions (c) and two LB films (b, d) under UV lamp irradiation.

present.[37] In Figure 7a, the NiFe-LDH/PAA-Azo infrared spectrum curve shows two peaks near 2925 and 2849 cm^{-1}, which represent the C−H bond stretching vibration peaks of $-CH_2$ and $-CH_3$. The peaks at 1635 and 1506 cm^{-1} are characteristic absorption peaks of the C═C skeleton of the benzene ring. The nitrogen−nitrogen double bond (N═N) characteristic stretching vibration peak is affected by the benzene ring, and the absorption peak appears at 1642 cm^{-1}. Similarly, the NiFe-LDH/N-Azo composite film shown in Figure 7b also exhibits specific peak wavelengths of the above-mentioned groups. These results further illustrate that the positively charged azo groups in PAA-Azo and N-Azo molecules can undergo hydrogen bonding and electrostatic interaction with the sulfonic acid group of NiFe-LDH, thereby changing the wavelength position of the N−H bond. It can be clearly seen in Figure 7a,b that the composite films also show the partial vibration absorption peak of the S═O bond, the benzene ring in the original material, and the vibration band of N═N. In summary, supramolecular self-assembly has been occurred between the azobenzene molecules and NiFe-LDH in the composite films.

2.2. Photoisomerization Analysis. Two kinds of subphases and their composite LB films were irradiated with a wavelength of 365 nm using an UV lamp in a dark environment, and the photoisomerization characteristics of the composite films were studied. For the PAA-Azo solution in Figure 8a, the characteristic peak of the $\pi-\pi^*$ transfer of the trans isomer at 341 nm rapidly decreased after 5 s of UV lamp irradiation. With an increase in the irradiation time, the peak position gradually blue-shifted and the absorption intensity decreased slowly and finally maintained at 328 nm. An intermediate with a certain degree of stability was produced in the process, and its formation was slow in the initial stage.[23] At the same time, a slightly enhanced peak at 438 nm represents the $n-\pi^*$ shift in cis isomerism. The reason for a red shift in the characteristic peak position with a decrease in the peak intensity may be the different contents of intermediates, the breaking of the N═N bond of some molecules, or the

https://dx.doi.org/10.1021/acsomega.9b04290
ACS Omega 2020, 5, 3689−3698

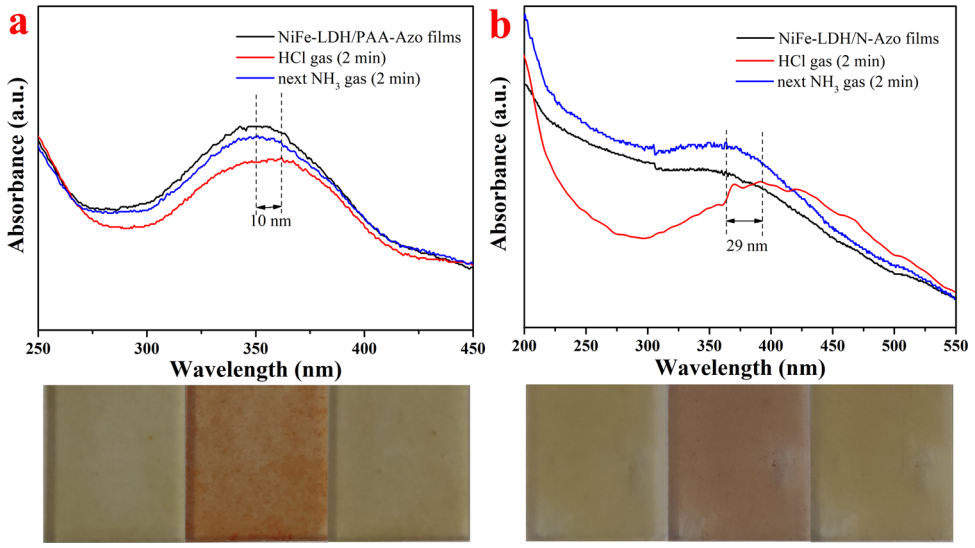

Figure 9. UV spectra and photos of the NiFe-LDH/PAA-Azo (a) and NiFe-LDH/N-Azo LB films (b) exposed to HCl and NH_3 gases (photos, from left to right, represent the original composite film, the film exposed to HCl, and next exposed to NH_3 gas, respectively).

intermolecular and molecular−solvent interactions. After cumulative irradiation for 60−120 s, the curves do not change any more, indicating that the state of the cis group in the solution tends to be stable and saturated. At this time, there are both trans and cis isomers in the solution.

The UV spectra of NiFe-LDH/PAA-Azo composite LB films under UV lamp irradiation are shown in Figure 8b. The peak at 351 nm had a significant downward trend when UV irradiation was performed for 20 s, and it remained almost unchanged after the irradiation time increased to 240 s. It shows that after PAA-Azo is combined to a composite film, the structure becomes more stable than before. The peak intensity does not change in a short time, which indicates that the trans−cis isomer of azobenzene reaches equilibrium. For the composite films of polarized NiFe-LDH and N-Azo (Figure 8d), the spectrum basically changed little after 5 min of light irradiation. The spectral intensity changes of the two composite films after light irradiation were relatively weak, which might be due to the better stability of the polarization film. In addition, the light stability of these films has been improved. At the same time, it is also reasonable that the azo groups recombine to form J-type aggregates on the surface of the NiFe-LDH sheet, and a certain steric hindrance occurs, which prevents the trans−cis isomerization process from occurring.[28,30] This phenomenon also coincides with the multiple characterization structures described earlier.

2.3. Acid−Base Gas Response Analysis. After exploring the light stability of the LB composite films, related acid−base gas induction tests were also performed. The changes in the characteristic peak positions of two different subphase NiFe-LDH composite films were analyzed in detail by UV−vis spectra. Figure 9a,b respectively shows the UV spectrum after 2 min of HCl gas and NH_3 gas treatment for NiFe-LDH/PAA-Azo and NiFe-LDH/N-Azo multilayer LB composite films. The pictures below the spectra correspond to the color contrast of the composite films before and after the acid−base gas atmosphere. Through observation and comparison, it was found that the two LB films were more sensitive to changes in the acid−base atmosphere. When the acid−base atmosphere changes, the original absorption peak corresponding to the film in the spectrum is red-shifted or blue-shifted.[38] It can be seen from Figure 9a that after contacting the HCl gas, the original peak of the NiFe-LDH/PAA-Azo film at about 351 nm was red-shifted by 10 nm. After full contact with NH_3 gas, the peak position returned to the vicinity of 351 nm. Similar to Figure 9a, after the HCl gas treatment, the position of the NiFe-LDH/N-Azo film peak in Figure 9b was also red-shifted by 29 nm. After the NH_3 treatment, the peak returned to almost the same position as the original position. At the same time, the initial color of the NiFe-LDH/PAA-Azo film is light brown to nearly transparent. Under a certain concentration of HCl gas, the color changes to orange-brown, and then under a certain concentration of NH_3 gas, the film gradually returns to its original color. The color of the NiFe-LDH/N-Azo film changes from the original light brown to reddish brown and finally converts back to light brown. It is worth noting that these changes occur very quickly and the color changes of films are very sensitive. These changes can be assigned to the presence of heteroatoms (such as N atoms) in the subphase solvents and film material structures with the changes in the external acid−base atmosphere.[30,37] As a result, the internal structure of the composite film changes, which affects the charge transfer.[39] That is, when the acidic gas contacts the thin films, the acidic medium undergoes a protonation reaction with the positively charged $-NH_2$ group in the film structure and then a deprotonation reaction occurs after contacting with the alkaline gas. The above conclusions showed that the dense and uniform composite films prepared by LB technology had acid−base discoloration properties, and the film materials have a high sensitivity for acid−base gas sensors.[40−48]

Finally, to facilitate the reuse of the LB composite films, after each contact with HCl and NH_3 gas, the films were soaked or rinsed with ultrapure water, and then the byproducts on the surface can be removed. Afterward, the next acid−base treatment can be performed again. After multiple cycles, combined with each measurement of the UV−vis spectrum data, the results after six cycles of two different LB composite films are shown in Figure 10. The ordinate shows the ratio of the ultraviolet maximum absorption intensities. Here, I_0 represents the maximum ultraviolet absorbance of the composite films in the initial state and I_n represents the maximum ultraviolet absorbance of the composite films after n

https://dx.doi.org/10.1021/acsomega.9b04290
ACS Omega 2020, 5, 3689−3698

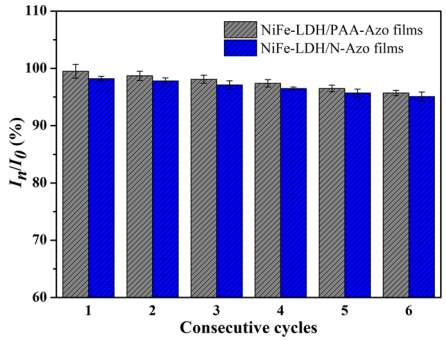

Figure 10. Stability characterization of NiFe-LDH/PAA-Azo and NiFe-LDH/N-Azo LB films.

cycles. The analysis results show that after six cycles of reaction, the UV intensity ratio is maintained at about 95%. Additionally, it shows that the prepared LB films have good recyclability, which also confirms that the prepared LB film materials have broad application prospects.[49−57]

3. CONCLUSIONS

In summary, new ordered NiFe-LDH/PAA-Azo and NiFe-LDH/N-Azo self-assembled composite films were successfully prepared by LB technology. In the LB composite film, the positively charged NiFe-LDH sheets can induce the subphase azo molecules to form J-type aggregates, thereby producing nanoscale uniform films with different morphologies. The characteristics of the LB composite films have also been characterized by various tests. The photoisomerization characteristics and acid−base gas response characteristics of the composite films were studied by UV−vis spectra. Under the UV light irradiation, the ultraviolet spectra of the two azobenzene solutions change significantly, whereas the two composite films change slowly or even unchanged. The above phenomenon is due to the NiFe-LDH and the azo groups on the LDH sheet surface forming an ordered stacked J-type aggregate with sterile hindrance, which hinders the trans−cis isomerization conversion. When the composite films were repeatedly cycled in the atmosphere of HCl and NH_3, the $-NH_2$ groups in LB films underwent a sensitive discoloration phenomenon (protonation and deprotonation) due to the change of acid−base atmosphere and the obtained composite films exhibited good recyclability. Therefore, the NiFe-LDH/PAA-Azo and NiFe-LDH/N-Azo composite films can be used as functional materials for light response and a gas sensor. The current work provides useful clues for the acid−base discoloration in self-assembled LB films and opens up new ideas for the study of photoresponsive materials and chemical gas sensor composites.

4. EXPERIMENTAL SECTION

4.1. Materials. $FeSO_4·9H_2O$ (≥99.5 wt %), $NiSO_4·6H_2O$ (≥98.5 wt %), methanol (CH_3OH), and ethanol (C_2H_5OH) were purchased from Sinopharm Chemical Reagent Co., Ltd. $CO(NH_2)_2$ and NH_4F were purchased from Qinhuangdao Reagent Factory of Hebei, China, and were of analytical reagent grade. Hydrochloric acid (HCl, 37 wt %) and ammonia ($NH_3·H_2O$, 25 wt %) were obtained from Tianjin Kaitong Industrial Chemical Reagent Company. 4-Aminoazobenzene (N-Azo) was purchased from Tianjin Alfa Aesar Chemical Reagent Factory. Polyacrylic acid (PAA; average molecular weight, 450 000) was purchased from Shanghai Aladdin Reagent Chemical Company. Polyacrylic acid azo derivative (PAA-Azo) was prepared according to the previous method. The experimental water was ultrapure water purified by the Milli-Q Plus system.

4.2. Preparation of NiFe-LDH. The route for the synthesis of raw materials was referred from a relative report.[58] Experimental conditions were adjusted to ensure operation under the proper conditions in this work. Under continuous stirring, 3.6 mmol of $NiSO_4·6H_2O$ and 1.8 mmol of $FeSO_4·9H_2O$ were dissolved in 50 mL of ultrapure water, and then 126 mmol of $CO(NH_2)_2$ and 20 mmol of NH_4F were added after 15 min. After the solid powder was sufficiently dissolved, the mixed solution was transferred to a 100 mL sealed autoclave, hydrothermally treated at 180 °C for 12 h, and then cooled to room temperature. The black product was centrifuged and washed with repeated alcohol and water procedures until neutral conditions. The finally obtained composite was freeze-dried at −50 °C.

4.3. Preparation of NiFe-LDH Langmuir Films. Before preparing the Langmuir films, it is necessary to thoroughly clean the LB trough with methanol and ultrapure water, and the diffusion solution (0.7 mg/mL, NiFe-LDH) is prepared in advance. The first step is to fill the trough with a subphase solution (three subphases are used here: ultrapure water, PAA-Azo, and N-Azo solutions with a concentration of 50 mg/L). The second step is to spread the prepared diffusion solution dropwise on the surface of the subphase solution with a microsyringe. Subsequently, after the methanol solvent evaporates for 20−25 min, the surface solvent and subphase solution fully interact to form a thin dense layer. Then, the film is transferred to different substrates under appropriate pressure, and the single-layer and multilayer LB films were finally obtained.

4.4. Photoisomerism and Gas Response Experiments. First, multilayer (at least 70 layers) composite LB films were selected, transferred to a quartz substrate, and irradiated it with an UV lamp at a wavelength of 365 nm. The changes in the internal configuration of the composite films were further investigated by UV−vis spectroscopy. Then, the obtained multilayer (at least 70 layers) composite LB films were exposed to HCl and NH_3 atmospheres, respectively. The color changes of the prepared films were monitored by UV−vis spectroscopy.

4.5. Characterization. The instrument model used to prepare or transfer the LB films for operation is the KSV-NIMA system (Purchased from Biolan Technology, Sweden). The microstructure of the product was depicted using a transmission electron microscope (TEM, HT7700, High-Technologies Corp., Ibaraki, Japan). Atomic force microscopy (AFM) images were obtained using a silicon cantilever probe microscope (Veeco Instrument), Nanoscope Model Multimode 8. X-ray diffraction (XRD, SMART LAB, Rigaku) was used to characterize the molecular orientation and microstructure of NiFe-LDH and composite films. To measure the FTIR spectrum using a Thermo Nicolet Corporation spectrometer, it is necessary to transfer the film layer-by-layer to the CaF_2 substrate in advance. After transferring the films to a quartz substrate, UV−visible spectroscopy (UV−vis) can be performed using the Shimadzu UV-2550 system. Photoisomerism and acid−base gas response phenomena can be characterized by UV−vis spectroscopy, and color changes can be obtained by taking a quartz plate with a Nikon (Tokyo) D90 A SLR camera.

https://dx.doi.org/10.1021/acsomega.9b04290
ACS Omega 2020, 5, 3689−3698

AUTHOR INFORMATION

Corresponding Authors

Lexin Zhang − *Hebei Key Laboratory of Applied Chemistry, Hebei Key Laboratory of Heavy Metal Deep-Remediation in Water and Resource Reuse, School of Environmental and Chemical Engineering, Yanshan University, Qinhuangdao 066004, P. R. China*; Email: zhanglexin@ysu.edu.cn

Tifeng Jiao − *Hebei Key Laboratory of Applied Chemistry, Hebei Key Laboratory of Heavy Metal Deep-Remediation in Water and Resource Reuse, School of Environmental and Chemical Engineering and State Key Laboratory of Metastable Materials Science and Technology, Yanshan University, Qinhuangdao 066004, P. R. China*; orcid.org/0000-0003-1238-0277; Email: tfjiao@ysu.edu.cn

Authors

Ying He − *Hebei Key Laboratory of Applied Chemistry, Hebei Key Laboratory of Heavy Metal Deep-Remediation in Water and Resource Reuse, School of Environmental and Chemical Engineering, Yanshan University, Qinhuangdao 066004, P. R. China*

Ran Wang − *Hebei Key Laboratory of Applied Chemistry, Hebei Key Laboratory of Heavy Metal Deep-Remediation in Water and Resource Reuse, School of Environmental and Chemical Engineering, Yanshan University, Qinhuangdao 066004, P. R. China*

Chenguang Sun − *National Engineering Research Center for Equipment and Technology of Cold Strip Rolling, Yanshan University, Qinhuangdao 066004, P. R. China*

Shufeng Liu − *Key Laboratory of Optic-electric Sensing and Analytical Chemistry for Life Science, Ministry of Education, College of Chemistry and Molecular Engineering, Qingdao University of Science and Technology, Qingdao 266042, P. R. China*; orcid.org/0000-0003-4063-4537

Jingxin Zhou − *Hebei Key Laboratory of Applied Chemistry, Hebei Key Laboratory of Heavy Metal Deep-Remediation in Water and Resource Reuse, School of Environmental and Chemical Engineering, Yanshan University, Qinhuangdao 066004, P. R. China*

Qiuming Peng − *State Key Laboratory of Metastable Materials Science and Technology, Yanshan University, Qinhuangdao 066004, P. R. China*; orcid.org/0000-0002-3053-7066

Complete contact information is available at: https://pubs.acs.org/10.1021/acsomega.9b04290

Notes

The authors declare no competing financial interest.

ACKNOWLEDGMENTS

This work was financially supported by the National Natural Science Foundation of China (No. 21872119), the Talent Engineering Training Funding Project of Hebei Province (No. A201905004), and the Research Program of the College Science and Technology of Hebei Province (No. ZD2018091).

REFERENCES

(1) Yu, L.; Deng, J.; Wang, H.; Liu, J.; Zhang, Y. Improved salts transportation of a positively charged loose nanofiltration membrane by introduction of poly (ionic liquid) functionalized hydrotalcite nanosheets. *ACS Sustainable Chem. Eng.* **2016**, *4*, 3292−3304.

(2) Zhang, Y.; Wang, H.; Zhang, Y.; Ding, X.; Liu, J. Thin film composite membranes functionalized with montmorillonite and hydrotalcite nanosheets for CO_2/N_2 separation. *Sep. Purif. Technol.* **2017**, *189*, 128−137.

(3) Chen, C.; Zeng, H.; Sun, Y.; Xu, S.; Du, J.; Xiao, G.; Shen, J. Facile Hydrothermal Preparation of Carboxymethyl Chitosan Functionalized Hydrotalcite Composite with Enhanced Adsorption Capacity for Cu (II) Ions. *J. Nanosci. Nanotechnol.* **2018**, *18*, 8225−8231.

(4) Navajas, A.; Campo, I.; Moral, A.; Echave, J.; Sanz, O.; Montes, M.; Odriozola, J. A.; Arzamendi, G.; Gandia, L. M. Outstanding performance of rehydrated Mg-Al hydrotalcites as heterogeneous methanolysis catalysts for the syntheseis of biodiesel. *Fuel* **2018**, *211*, 173−181.

(5) Sakthivel, A.; Mahato, N. R.; Baskaran, T.; Christopher, J. Molybdenum carbonyl grafted onto silicate intercalated cobalt−aluminum hydrotalcite: A new potential catalyst for the hydroformylation of octene. *Catal. Commun.* **2015**, *65*, 55−61.

(6) Yang, X. J.; Zhang, P.; Li, P.; Li, Z.; Xia, W.; Zhang, H.; Di, Z.; Wang, M.; Zhang, H.; Niu, Q. J. Layered double hydroxide/polyacrylamide nanocomposite hydrogels: Green preparation, rheology and application in methyl orange removal from aqueous solution. *J. Mol. Liq.* **2019**, *280*, 128−134.

(7) Wang, X.; Wang, H.; Wang, Y.; Gao, J.; Liu, J.; Zhang, Y. Hydrotalcite/graphene oxide hybrid nanosheets functionalized nanofiltration membrane for desalination. *Desalination* **2019**, *451*, 209−218.

(8) Chakraborty, A.; Acharya, H. Facile synthesis of MgAl-layered double hydroxide supported metal organic framework nanocomposite for adsorptive removal of methyl orange dye. *J. Colloid Interface Sci.* **2018**, *24*, 35−39.

(9) Wang, R.; Yu, Q.; He, Y.; Bai, J.; Jiao, T.; Zhang, L.; Bai, Z.; Zhou, J.; Peng, Q. Self-assembled polyelectrolyte-based composite hydrogels with enhanced stretchable and adsorption performances. *J. Mol. Liq.* **2019**, *294*, No. 111576.

(10) Posati, T.; Latterini, L.; Cipiciani, A.; Benfenati, V.; Zamboni, R.; Muccini, M.; Nocchetti, M. An Overview on the Different Approaches to Obtain Luminescent Hydrotalcite Nanoparticles and Films. *Curr. Phys. Chem.* **2016**, *5*, 173−184.

(11) Neporent, B. S.; Stolbova, O. V. The Orientation Photodichroism of Viscous Solutions. *Opt. Spectrosc.* **1961**, *10*, 146.

(12) Natansohn, A.; Xie, S.; Rochon, P. Azo polymers for reversible optical storage. 2. Poly [4′-[[2-(acryloyloxy) ethyl] ethylamino]-2-chloro-4-nitroazobenzene. *Macromolecules* **1992**, *25*, 5531−5532.

(13) Kharintsev, S. S.; Chernykh, E. A.; Fishman, A. I.; Saikin, S. K.; Alekseev, A. M.; Salakhov, M. K. Photoinduced heating of freestanding azo-polymer thin films monitored by scanning thermal microscopy. *J. Phys. Chem. C* **2017**, *121*, 3007−3012.

(14) Lacroix, P. G.; Malfant, I.; Lepetit, C. Second-order nonlinear optics in coordination chemistry: an open door towards multifunctional materials and molecular switches. *Coord. Chem. Rev.* **2016**, *308*, 381−394.

(15) Zhou, X.; Du, Y.; Wang, X. Azo polymer janus particles and their photoinduced, symmetry-breaking deformation. *ACS Macro Lett.* **2016**, *5*, 234−237.

(16) Shen, J.; Xin, X.; Liu, G.; Pang, J.; Song, Z.; Xu, G.; Yuan, S. Fabrication of smart pH-responsive fluorescent solid-like giant vesicles by ionic self-assembly strategy. *J. Phys. Chem. C* **2016**, *120*, 27533−27540.

(17) Xia, C.; Zhang, S.; Sun, D.; Jiang, B.; Wang, W.; Xin, X. Coassembly of Mixed Weakley-Type Polyoxometalates to Novel Nanoflowers with Tunable Fluorescence for the Detection of Toluene. *Langmuir* **2018**, *34*, 6367−6375.

(18) Xia, C.; Wang, Z.; Sun, D.; Jiang, B.; Xin, X. Hierarchical nanostructures self-assembled by polyoxometalate and alkylamine for photocatalytic degradation of dye. *Langmuir* **2017**, *33*, 13242−13251.

(19) Kumar, K. D. A.; Ganesh, V.; Shkir, M.; AlFaify, S.; Valanarasu, S. Effect of different solvents on the key structural, optical and electronic properties of sol−gel dip coated AZO nanostructured thin films for optoelectronic applications. *J. Mater. Sci.: Mater. Electron.* **2018**, *29*, 887−897.

(20) Karthika, M.; Chi, H.; Li, T.; Wang, H.; Thomas, S. Superhydrophobic graphene oxide-azobenzene hybrids for improved hydrophobicity of polyurethane. *Composites, Part B* **2019**, No. 106978.
(21) Boussoualem, Y.; Ismaili, M.; Daoudi, A. Photo enhancement of spontaneous polarization in ferroelectric liquid crystal doped with azo-molecules. *Appl. Phys. Lett.* **2015**, *107*, No. 112902.
(22) Pirani, F.; Angelini, A.; Ricciardi, S.; Frascella, F.; Descrovi, E. Laser-induced anisotropic wettability on azopolymeric microstructures. *Appl. Phys. Lett.* **2017**, *110*, No. 101603.
(23) Zubizarreta, C.; G-Berasategui, E.; Ciarsolo, I.; Barriga, J.; Gaspar, D.; Martins, R.; Fortunato, E. The influence of target erosion grade in the optoelectronic properties of AZO coatings growth by magnetron sputtering. *Appl. Surf. Sci.* **2016**, *380*, 218−222.
(24) Kulyk, B.; Guichaoua, D.; Ayadi, A.; El-Ghayoury, A.; Sahraoui, B. Metal-induced efficient enhancement of nonlinear optical response in conjugated azo-based iminopyridine complexes. *Org. Electron.* **2016**, *36*, 1−6.
(25) Wang, L.; Zhang, Y.; Zhan, C.; You, Y.; Zhang, H.; Ma, J.; Xiong, Z.; Liu, X.; Wei, R. Synthesis and Photoinduced Anisotropy of Polymers Containing Nunchaku-Like Unit with an Azobenzene and a Mesogen. *Polymers* **2019**, *11*, 600.
(26) Shen, J.; Xin, X.; Liu, T.; Wang, S.; Yang, Y.; Luan, X.; Xu, G.; Yuan, S. Ionic self-assembly of a giant vesicle as a smart microcarrier and microreactor. *Langmuir* **2016**, *32*, 9548−9556.
(27) Song, Z.; Xin, X.; Shen, J.; Zhang, H.; Wang, S.; Yang, Y. Reversible controlled morphologies switching between porous microspheres and urchin-like microcrystals for NaDC/RhB self-assembly and their multifunctional applications. *J Mater. Chem. C* **2016**, *4*, 8439−8447.
(28) Gao, Y.; Jiao, T.; Ma, K.; Xing, R.; Zhang, L.; Zhou, J.; Peng, Q. Variable self-assembly and in situ host−guest reaction of beta-cyclodextrin-modified graphene oxide composite Langmuir films with azobenzene compounds. *RSC Adv.* **2017**, *7*, 41043−41051.
(29) Holm, A.; Kunz, L.; Riscoe, A. R.; Kao, K. C.; Cargnello, M.; Frank, C. W. General Self-Assembly Method for Deposition of Graphene Oxide into Uniform Close-Packed Monolayer Films. *Langmuir* **2019**, *35*, 4460−4470.
(30) He, Y.; Wang, R.; Jiao, T.; Yan, X.; Wang, M.; Zhang, L.; Bai, Z.; Zhang, Q.; Peng, Q. Facile Preparation of Self-Assembled Layered Double Hydroxide-Based Composite Dye Films as New Chemical Gas Sensors. *ACS Sustainable Chem. Eng.* **2019**, *7*, 10888−10899.
(31) Lawrence, A. S. C.; Bingham, A.; Capper, C. B.; Hume, K. The penetration of water and aqueous soap solutions into fatty substances containing one or two polar groups. *J. Phys. Chem. A.* **1964**, *68*, 3470−3476.
(32) Reeves, R. L.; Kaiser, R. S. Selective solvation of hydrophobic ions in structured solvents. Azo-hydrazone tautomerism of azo dyes in aqueous organic solvents. *J. Org. Chem.* **1970**, *35*, 3670−3675.
(33) Liu, G.; Yuan, Q.; Hollett, G.; Zhao, W.; Kang, Y.; Wu, J. Cyclodextrin-based host-guest supramolecular hydrogel and its application in biomedical fields. *Polym. Chem.* **2018**, *9*, 3436−3449.
(34) Tippmann-Krayer, P.; Moehwald, H. Precise determination of tilt angles by x-ray diffraction and reflection with arachidic acid monolayers. *Langmuir* **1991**, *7*, 2303−2306.
(35) Hu, Z.; Chen, G. Novel nanocomposite hydrogels consisting of layered double hydroxide with ultrahigh tensibility and hierarchical porous structure at low inorganic content. *Adv. Mater.* **2014**, *26*, 5950−5956.
(36) Dähne, L.; Biller, E. Color variation in highly oriented dye layers by polymorphism of dye aggregates. *Adv. Mater.* **1998**, *10*, 241−245.
(37) Sun, S.; Wang, C.; Han, S.; Jiao, T.; Wang, R.; Yin, J.; Li, Q.; Wang, Y.; Geng, L.; Yu, X.; Peng, Q. Interfacial nanostructures and acidichromism behaviors in self-assembled terpyridine derivatives Langmuir-Blodgett films. *Colloids Surf., A* **2019**, *564*, 1−9.
(38) Liu, Y.; Zhang, Y.; Wu, X.; Lan, Q.; Chen, C.; Liu, S.; Chen, X.; Chi, Z.; Jiang, L.; Xu, J. Deep-blue luminescent compound that emits efficiently both in solution and solid state with considerable blue-shift upon aggregation. *J. Mater. Chem. C* **2014**, *2*, 1068−1075.
(39) Zhang, J.; Chen, J.; Xu, B.; Wang, L.; Ma, S.; Dong, Y.; Li, B.; Ye, L.; Tian, W. Remarkable fluorescence change based on the protonation-deprotonation control in organic crystals. *Chem. Commun.* **2013**, *49*, 3878−3880.
(40) Cai, C.; Wang, R.; Liu, S.; Yan, X.; Zhang, L.; Wang, M.; Tong, Q.; Jiao, T. Synthesis of Self-Assembled Phytic Acid-MXene Nanocomposites via a Facile Hydrothermal Approach with Elevated Dye Adsorption Capacities. *Colloids Surf., A* **2020**, *589*, No. 124468.
(41) Xu, Y.; Wang, R.; Zheng, Y.; Zhang, L.; Jiao, T.; Peng, Q.; Liu, Z. Facile Preparation of Self-Assembled Ni/Co Phosphates Composite Spheres with Highly Efficient HER Electrocatalytic Performances. *Appl. Surf. Sci.* **2020**, *509*, No. 145383.
(42) Geng, R.; Yin, J.; Zhou, J.; Jiao, T.; Feng, Y.; Zhang, L.; Chen, Y.; Bai, Z.; Peng, Q. In Situ Construction of Ag/TiO_2/g-C_3N_4 Heterojunction Nanocomposite Based on Hierarchical Co-Assembly with Sustainable Hydrogen Evolution. *Nanomaterials* **2020**, *10*, 1.
(43) Zhan, F.; Yin, J.; Zhou, J.; Jiao, T.; Zhang, L.; Xia, M.; Bai, Z.; Peng, Q. Facile preparation and highly efficient catalytic performances of Pd-Cu bimetallic catalyst synthesized via Seed-mediated method. *Nanomaterials* **2020**, *10*, 6.
(44) Feng, Y.; Wang, R.; Yin, J.; Zhan, F.; Chen, K.; Jiao, T.; Zhou, J.; Zhang, L.; Peng, Q. Facile Synthesis of Cu_2O nanoparticle-loaded Carbon Nanotubes Composite Catalysts for Reduction of 4-Nitrophenol. *Curr. Nanosci.* **2019**, DOI: 10.2174/1573413715666191206161555.
(45) Li, H.; Yin, J.; Meng, Y.; Liu, S.; Jiao, T. Nickel/Cobalt-Containing Polypyrrole Hydrogel-Derived Approach for Efficient ORR Electrocatalyst. *Colloid Surf., A* **2020**, *586*, No. 124221.
(46) Zhao, J.; Yin, J.; Zhong, J.; Jiao, T.; Bai, Z.; Wang, S.; Zhang, L.; Peng, Q. Facile preparation of a self-assembled artemia cyst shell−TiO_2−MoS_2 porous composite structure with highly efficient catalytic reduction of nitro compounds for wastewater treatment. *Nanotechnology* **2020**, *31*, No. 085603.
(47) Meng, Y.; Yin, J.; Jiao, T.; Bai, J.; Zhang, L.; Su, J.; Liu, S.; Bai, Z.; Cao, M.; Peng, Q. Self-assembled copper/cobalt-containing polypyrrole hydrogels for highly efficient ORR electrocatalysts. *J. Mol. Liq.* **2020**, *298*, No. 112010.
(48) Yin, J.; Zhan, F.; Jiao, T.; Deng, H.; Zou, G.; Bai, Z.; Zhang, Q.; Peng, Q. Highly efficient catalytic performances of nitro compounds via hierarchical PdNPs-loaded MXene/polymer nanocomposites synthesized through electrospinning strategy for wastewater treatment. *Chin. Chem. Lett.* **2020**, DOI: 10.1016/j.cclet.2019.08.047.
(49) Ma, K.; Wang, R.; Jiao, T.; Zhou, J.; Zhang, L.; Li, J.; Bai, Z.; Peng, Q. Preparation and aggregate state regulation of co-assembly graphene oxide-porphyrin composite Langmuir films via surface-modified graphene oxide sheets. *Colloid Surf., A* **2020**, *584*, No. 124023.
(50) Zhu, J.; Wang, R.; Geng, R.; Zhang, X.; Wang, F.; Jiao, T.; Yang, J.; Bai, Z.; Peng, Q. A facile preparation method for new two-component supramolecular hydrogels and their performances in adsorption, catalysis, and stimuli-response. *RSC Adv.* **2019**, *9*, 22551−22558.
(51) Hou, N.; Wang, R.; Geng, R.; Wang, F.; Jiao, T.; Zhang, L.; Zhou, J.; Bai, Z.; Peng, Q. Facile Preparation of Self-Assembled Hydrogels Constructed by Poly-Cyclodextrin and Poly-Adamantane as Highly Selective Adsorbents for Wastewater Treatment. *Soft Matter* **2019**, *15*, 6097−6106.
(52) Wang, C.; Yin, J.; Han, S.; Jiao, T.; Bai, Z.; Zhou, J.; Zhang, L.; Peng, Q. Preparation of Palladium Nanoparticles Decorated Polyethyleneimine/Polycaprolactone Composite Fibers Constructed by Electrospinning with Highly Efficient and Recyclable Catalytic Performances. *Catalysts* **2019**, *9*, 559.
(53) Ma, K.; Chen, W.; Jiao, T.; Jin, X.; Sang, Y.; Yang, D.; Zhou, J.; Liu, M.; Duan, P. Boosting Circularly Polarized Luminescence of Small Organic Molecules via Multi-dimensional Morphology Control. *Chem. Sci.* **2019**, *10*, 6821−6827.

https://dx.doi.org/10.1021/acsomega.9b04290
ACS Omega 2020, 5, 3689−3698

(54) Yuan, J.; Liu, M. Chiral molecular assemblies from a novel achiral amphiphilic 2-(heptadecyl) naphtha [2,3] imidazole through interfacial coordination. *J. Am. Chem. Soc.* **2003**, *125*, 5051−5056.
(55) Huang, X.; Li, C.; Jiang, S. G.; Wang, X. S.; Zhang, B. W.; Liu, M. H. Self-assembled spiral nanoarchitecture and supramolecular chirality in Langmuir-Blodgett films of an achiral amphiphilic barbituric acid. *J. Am. Chem. Soc.* **2004**, *126*, 1322−1323.
(56) Qiu, Y. F.; Chen, P. L.; Liu, M. H. Evolution of various porphyrin nanostructures via an oil/aqueous medium: controlled self-assembly, further organization, and supramolecular chirality. *J. Am. Chem. Soc.* **2010**, *132*, 9644−9652.
(57) Guo, P. Z.; Zhang, L.; Liu, M. H. A supramolecular chiroptical switch exclusively from an achiral amphiphile. *Adv. Mater.* **2006**, *18*, 177−180.
(58) Wang, Y.; Jiang, C.; Le, Y.; Cheng, B.; Yu, J. Hierarchical honeycomb-like Pt/NiFe-LDH/rGO nanocomposite with excellent formaldehyde decomposition activity. *Chem. Eng. J.* **2019**, *365*, 378−388.

https://dx.doi.org/10.1021/acsomega.9b04290
ACS Omega 2020, 5, 3689−3698